# Passive Nonreciprocity in a System of Asymmetrical Rotational Oscillators

Lezheng Fang,[1] Alireza Mojahed,[2] Amir Darabi,[1,2] Alexander F. Vakakis,[2] and Michael J. Leamy[1,*]

[1] *George W. Woodruff School of Engineering, Georgia Institute of Technology, Atlanta, Georgia, USA*
[2] *Department of Mechanical Science and Engineering, University of Illinois at Urbana-Champaign, Champaign, Illinois, USA*

(Received 22 October 2020; revised 28 December 2020; accepted 1 February 2021; published 2 March 2021)

In this paper we investigate an elastically linked, nonlinear, in-plane rotator system and experimentally study its nonreciprocal impulse response. The nonlinearity of the system arises from the angled elastic linkage in rotational motion. A chain of rotators coupled with such linkages reaches an acoustic vacuum when the pretension of the elastic links vanish, leading to large nonlinearity tunable via small pretension. Using an analytical model and experimental exploration, we observe a broadband nonreciprocity in a weakly pretensioned, asymmetric, three-rotator system. In addition, we use a nonlinear normal-mode (NNM) analysis, capturing the main qualitative dynamics of the response, to explain the observed nonreciprocity mechanism. The analysis shows that equal applied impulses, combined with energy-dependent frequency and mode shapes, result in robust nonreciprocity features, contrary to the reciprocal response present in the linear counterpart of this system.

DOI: 10.1103/PhysRevApplied.15.034005

## I. INTRODUCTION

Reciprocity, a fundamental property of linear time-invariant systems, ensures an identical response when a source and receiver interchange position [1–3]. Breaking reciprocity, due to its large potential in applications such as targeted energy transfer [4–8], wave transmission control [9–17], and signal filtering and protection [18–20], has attracted increased recent attention. In acoustic and elastic media, *active* means breaking reciprocity by adopting odd-symmetry field and circulation [12,15,21], time-modulated materials [13,18,22–26], and external control [27–29], as reviewed in Ref. [30]. However, these active methods, due to their complexity and external dependencies, raise concerns about instability and energy consumption for practical implementation [27].

An alternative for achieving nonreciprocity relies on nonlinear mechanisms and system asymmetry, which can be realized in a *passive* manner and thus avoid the aforementioned shortcomings of active systems. In general, a nonlinear system may not break reciprocity or behave in a nonreciprocal fashion, particularly when the system's symmetry is maintained. Li *et al.* leveraged nonlinearity-induced higher harmonics to bypass the band gap of a superlattice in one direction [10,11]. Other researchers utilized nonlinear bifurcations in a variety of systems to break reciprocity [5,28,31,32]. In phononic structures, nonlinear propagation zones in both weakly and strongly nonlinear lattices exhibit direction dependency due to asymmetry, leading to tunable nonreciprocity [19,33–36]. In low-degree-of-freedom nonlinear systems, a new nonreciprocity mechanism has been identified, which occurs due to nonlinear resonance and targeted energy transfer [6]. However, this mechanism requires symmetry breaking by a boundary nonlinear energy sink, which needs to be ungrounded and free to oscillate from one end of the lattice, restricting its generality.

Inspired by Refs. [6,37,38], in this paper we propose an asymmetric, lightly pretensioned, three-rotator system exhibiting passive nonreciprocity due to strong geometric nonlinearity. We show that the geometric nonlinearity in the system is tunable to the pretension of the elastic couplings, whose absence leads to an acoustic vacuum [37,39]. Using this system, we uncover a new, broadly applicable passive mechanism that passively breaks acoustic reciprocity. The simple three-rotator system exhibits broadband nonreciprocity in experimental tests, which agrees well with results from direct numerical simulation of an associated analytical model. Unlike nonreciprocity mechanisms featuring nonlinear resonance or bifurcation, we show that the observed nonreciprocal response arises from energy-dependent nonlinear normal modes (NNMs) intrinsic to the unit cell. Further, interpreting nonlinear nonreciprocity using NNM analysis suggests a new tool for exploring nonreciprocity in nonlinear media, which can be

*michael.leamy@me.gatech.edu

 

extrapolated to a class of nonlinear nonreciprocal problems where excitations induce distinct energies.

## II. SYSTEM DESCRIPTION

Figure 1(a) depicts three in-plane rotators linked by linear springs at their arms. Each rotator, with identical arm length, is pinned at its center and allows only rotational motion. The massless spring deforms only in its axial direction. The system is scaled by a moment of inertia hierarchy $I_1 < I_2 < I_3$. In this paper, we consider only small-angle oscillations around the equilibrium under the condition $L_i \leq D_i$ [i.e., each spring is either pretensioned or unstretched at the position shown in Fig. 1(a)]. Further, we define the angular displacement for these rotators counterclockwise positive, as shown in Fig. 1(b).

We next present the rotators' equations of motion. Each rotator is subject to a restoring and dissipation torque,

$$I_1\ddot{\boldsymbol{\theta}}_1 - \mathbf{T}_{1,2} - \mathbf{T}_1 = 0, \tag{1}$$

$$I_2\ddot{\boldsymbol{\theta}}_2 - \mathbf{T}_{2,1} - \mathbf{T}_{2,3} - \mathbf{T}_2 = 0, \tag{2}$$

$$I_3\ddot{\boldsymbol{\theta}}_3 - \mathbf{T}_{3,2} - \mathbf{T}_3 = 0, \tag{3}$$

where $\mathbf{T}_{i,j}$ describes the restoring torque on the rotator resulting from the elastic linkage between the $i$th and $j$th rotators, and $\mathbf{T}_i$ denotes the equivalent dissipation torque on the $i$th rotator. Due to the rotation, the rotator arm stretches the elastic linkage along an angle, and the restoring torque becomes nonproportional to the elastic linkage deformation. We derive the restoring torque from the rotation geometry,

$$\mathbf{r}_i = r\cos(\theta_i)i + r\sin(\theta_i)j\ , \tag{4}$$

$$\mathbf{r}_j = r\cos(\theta_j)i + r\sin(\theta_j)j\,, \tag{5}$$

$$L = (2r + D_{i^*})i\ - \mathbf{r}_1 - \mathbf{r}_2, \tag{6}$$

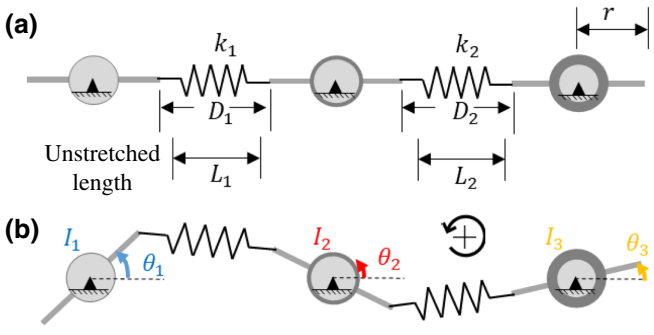


FIG. 1. System description. (a) Depiction of three in-plane rotators at the equilibrium position with system parameters marked. (b) Depiction at arbitrary angular displacement indicating the angular measures and spring stretch.

$$\Delta L = |\mathbf{L}| - L_{i^*}, \tag{7}$$

$$\mathbf{T}_{i,j} = \mathbf{r}_i \times \left(k_{i^*}\Delta L\frac{\mathbf{L}}{|\mathbf{L}|}\right), \tag{8}$$

where $i,j$ denotes the indices of two adjacent rotators, and $i^* = \min(i,j)$ is used to describe the parameters associated with the linkage between the $i$th and $j$th rotator. Vectors $\mathbf{r}$ and $\mathbf{L}$ then represent the angular positon of the rotator and stretch of the linkage, respectively. Guided by experimental observations, we model the dissipation torque as a combination of linear viscous damping and Coulomb friction with viscous coefficient $c_i$ and frictional torque $\mathbf{T}_{if}$,

$$\mathbf{T}_i = -c_i\dot{\boldsymbol{\theta}}_i - \mathrm{sgn}(\theta_i)\mathbf{T}_{if}\,. \tag{9}$$

Since we are interested in small-angle oscillations, we introduce a small parameter $\epsilon \ll 1$ to scale the angular displacements, $\theta_i \to \epsilon\theta_i$, and express the governing equations in a Taylor series with respect to $\epsilon$,

$$\begin{aligned} &I_1\ddot{\theta}_1 + [k_{g1}\theta_1 + k_{12}(\theta_1+\theta_2)]\epsilon \\ &\quad + \left[\gamma_{12}^{+}(\theta_1+\theta_2)^3 + \gamma_{12}^{-}(\theta_1-\theta_2)^3 + \gamma_{g1}\theta_1^3\right]\epsilon^3 + O(\epsilon^5) \\ &\quad + c_1\dot{\theta}_1 + \mathrm{sgn}(\theta_1)T_{1f} = 0, \end{aligned} \tag{10}$$

$$\begin{aligned} &I_2\ddot{\theta}_2 + [k_{g2}\theta_2 + k_{12}(\theta_1+\theta_2) + k_{23}(\theta_2+\theta_3)]\epsilon \\ &\quad + \left[\gamma_{12}^{+}(\theta_1+\theta_2)^3 + \gamma_{23}^{+}(\theta_2+\theta_3)^3 + \gamma_{12}^{-}(\theta_2-\theta_1)^3\right. \\ &\quad \left. + \gamma_{23}^{-}(\theta_2-\theta_3)^3 + \gamma_{g2}\theta_2^3\right]\epsilon^3 + O(\epsilon^5) \\ &\quad + c_2\dot{\theta}_2 + \mathrm{sgn}(\theta_2)T_{2f} = 0, \end{aligned} \tag{11}$$

$$\begin{aligned} &I_3\ddot{\theta}_3 + \left[k_{g3}\theta_3 + k_{23}(\theta_2+\theta_3)\right]\epsilon \\ &\quad + \left[\gamma_{23}^{+}(\theta_2+\theta_3)^3 + \gamma_{23}^{-}(\theta_3-\theta_2)^3 + \gamma_{g3}\theta_3^3\right]\epsilon^3 + O(\epsilon^5) \\ &\quad + c_3\dot{\theta}_3 + \mathrm{sgn}(\theta_3)T_{3f} = 0, \end{aligned} \tag{12}$$

where the linear stiffness $k_{gi}$, $k_{ij}$, and nonlinear stiffness $\gamma_{ij}^{+}$, $\gamma_{ij}^{-}$, and $\gamma_{gi}$ are functions of the system parameters—the Appendix provides complete expressions for each. Note that the linear stiffnesses $k_{gi}$ and $k_{ij}$ are both proportional to the pretension of the springs $(D_i - L_i)$.

Equations (10)–(12) document that (i) the system contains only odd (hardening) nonlinearities, and (ii) its linear stiffness can be modified or eliminated by adjusting or removing the pretensions of the springs. In both linear and cubic terms, the restoring torque depends on the sum of angular displacement, $\theta_i + \theta_j$, unlike rectilinear counterparts, which depend on displacement differences. In fact, this subtle difference results in a qualitative difference in the wave-propagation problem in a periodic structure composed of such rotator structures. See Supplemental Material [40] for an extended discussion.

## III. EXPERIMENTAL RESULTS

Figure 3(a) depicts three three-dimensionally printed rotators, each with radius 28.5 mm, attached to low-friction bearings affixed to a vibration isolation table. By varying the quantity of nuts and bolts attached to each rotator, an asymmetrical moment of inertia distribution can be introduced. In the designed experiment, from left to right, the rotators have inertia, $3.45 \times 10^{-6}$, $1.28 \times 10^{-5}$, and $3.16 \times 10^{-5}$ kg m$^2$, respectively. As illustrated in Fig. 3(b), the elastic linkage between two adjacent rotators consists of a weakly pretensioned short spring and two metal rings, which allows for axial extension and prevents spring bending. These elements have negligible mass compared to the three rotators and are all sufficiently lubricated. We perform a system identification study utilizing the *patternsearch* function in MATLAB (detailed within the Supplemental Material [40]) to accurately match the physical experiment to our analytical model, which employs MATLAB's ODE45 function to numerically integrate the governing equations. We present the identified experimental parameters below in Table I.

We use an impact hammer to strike a rotator arm at either end of the chain using the same impulse level. The

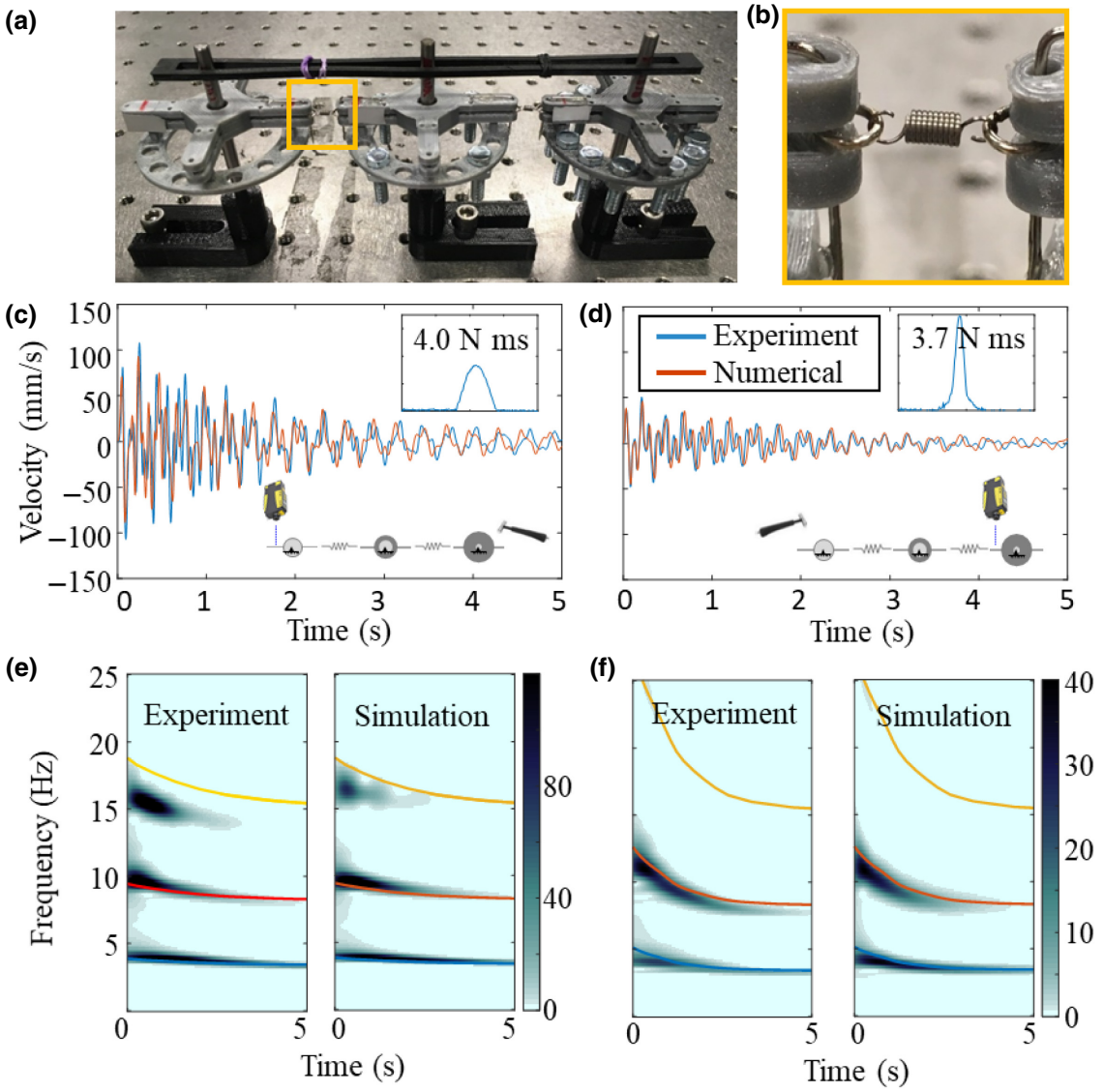


FIG. 2. Experimental and numerical nonreciprocity results. (a) Experimental setup used in testing, (b) detailed view of the spring connection, (c) time response (numerical and experimental) of the small (left) rotator when excitation is applied on the right. The impact (force in N versus time in ms) is documented in the top right corner, (d) time response (numerical and experimental) of the large (right) rotator, when the excitation is applied on the left. The impact is again plotted in the top right corner, (e) and (f) wavelet transformation (shaded) of the time responses shown in (c) and (d), superimposed by the nonlinear normal modes (solid lines) of the system.

impacts are carefully applied at roughly the same distance from the center of the rotator such that the angular impulses are equal. We then use a laser Doppler vibrometer to capture the response at the other end of the chain. As such, we present the experimental nonreciprocal response in Figs. 2(c)–2(f), at an impulse level $P \approx 3.85 \pm 0.15$ Nms, obtained from direct integration of experimental force responses, as depicted in the inscribed figures. It is noteworthy that, though the two impact excitations are not precisely the same (as shown in the inset figures), the impulse levels of two excitations are sufficiently close such that the contribution to reciprocity breaking from nonidentical excitations is negligible compared to the nonlinear effects we present, as substantiated in the Supplemental Material [40].

In Figs. 2(c) and 2(d), the experimental responses show a high degree of agreement with the superimposed numerical simulation results. We observe a large response at the left rotator when the impact excites the right rotator, compared to a smaller response at the right rotator when exciting the left rotator. A roughly 2:1 amplitude ratio appears in both experimental and numerical results. Results from a wavelet transformation performed on the experimental and numerical responses are displayed in Figs. 2(e) and 2(f), respectively. The wavelet results clarify the strong nonreciprocity in the frequency domain. Three dominant harmonics in the left-rotator response show considerable amplitude when the right rotator is excited, yet only two such harmonics appear in the right-rotator response when the impulse is applied on the left.

## IV. NONLINEAR NORMAL-MODE ANALYSIS

In order to better illustrate the dynamics of the system and interpret the nonreciprocal phenomenon, we apply a nonlinear normal-mode analysis to the three-degrees-of-freedom geometrically nonlinear system. Similar to linear normal modes (LNMs), NNMs depict periodic solutions of the nonlinear ordinary differential equations, yet in an energy-dependent framework. As defined by Shaw and Pierre in Refs. [41,42], a NNM is a two-dimensional invariant manifold in phase space, where an orbit starting on the manifold stays on the manifold for all time. At low-energy limits, the NNM manifold is tangent to the corresponding LNM, which is represented by a plane in the phase space. Different from the displacement ratio in the linear mode-shape concept, each NNM prescribes specific displacements for each degree of freedom, and hence a specific energy level for the entire system. We use the Newmark method and a continuation algorithm to numerically compute the NNMs, as detailed in Refs. [43–45], keeping only terms up to $O(\epsilon^5)$ in Eqs. (10)–(12). The energy-sensitive NNM can then be well illustrated in a frequency-energy plot accompanied with specific nonlinear mode shapes, which are the major focus of the following analysis.

In Fig. 3(a), three NNM branches emerge, each of them exhibiting increasing frequency with increasing modal energy. To verify with experimental and numerical results, we compute the instantaneous energy of the system at each time, and then replace the energy axis of Fig. 3(a) with time. The resultant plot is then superimposed on Figs. 2(e) and 2(f), where we find a high degree of agreement between the frequency evolution and NNM trajectories. Note that the experimental and numerical frequency branches are expected to be lower than the NNM results, since the dynamics composed of multiple NNMs (in our case, three) must have a total energy no less than the energy of each composed NNM. Conversely, the energy of each NNM in the presented dynamics must be lower than the total energy of the system as captured in simulations and experiments. In a hardening nonlinear system, a lower energy leads to a lower frequency, as also illustrated in Fig. 3(a).

The energy-dependent dynamics uncovered by the NNM analysis is key to understanding the nonreciprocal dynamics. In the studied system, due to the moment of inertia difference of the excited rotator, the same level of inputted impulse results in distinct initial energy ($E = P^2/2I_i$) inputted to the system. As indicated by the dashed lines in Fig. 3(a), the excitation on the left rotator (small moment of inertia) results in a larger initial energy (green dashed line) than the energy (purple dashed line) resulting from excitation on the right rotator (large moment of inertia). From these starting energies, dissipation then drives the response frequency leftwards to the low-energy regime in Fig. 3(a). As such, the responses are associated with nonidentical oscillation frequencies, which breaks reciprocity in the frequency domain, and matches the observations in Figs. 2(e) and 2(f).

Moreover, the nonlinearity not only generates the aforementioned frequency variation, but also leads to different nonlinear mode shapes for each excitation event. Figures 3(b)–3(g) illustrate the nonlinear normal mode shapes for each mode at two different energy levels (purple and green). Despite the difference in the amplitude of modal displacement (nonlinear normal modes are energy dependent, and cannot be normalized), the modes are fundamentally dissimilar at the given two energy levels. In the second mode [Figs. 3(c) and 3(f)], the modal displacement of the large rotator (rotator 3) is out of phase with respect to the small rotator (rotator 1) at low energy, yet becomes in-phase with the small rotator at high energy. Similarly, in the third mode, the modal displacement of the medium rotator (rotator 2) changes its sign at two energy levels as indicated in Figs. 3(d) and 3(g).

In Fig. 4 we present the modal participation of these NNMs as predicted by the numerical model. We superimpose the NNMs on the wavelet results for each

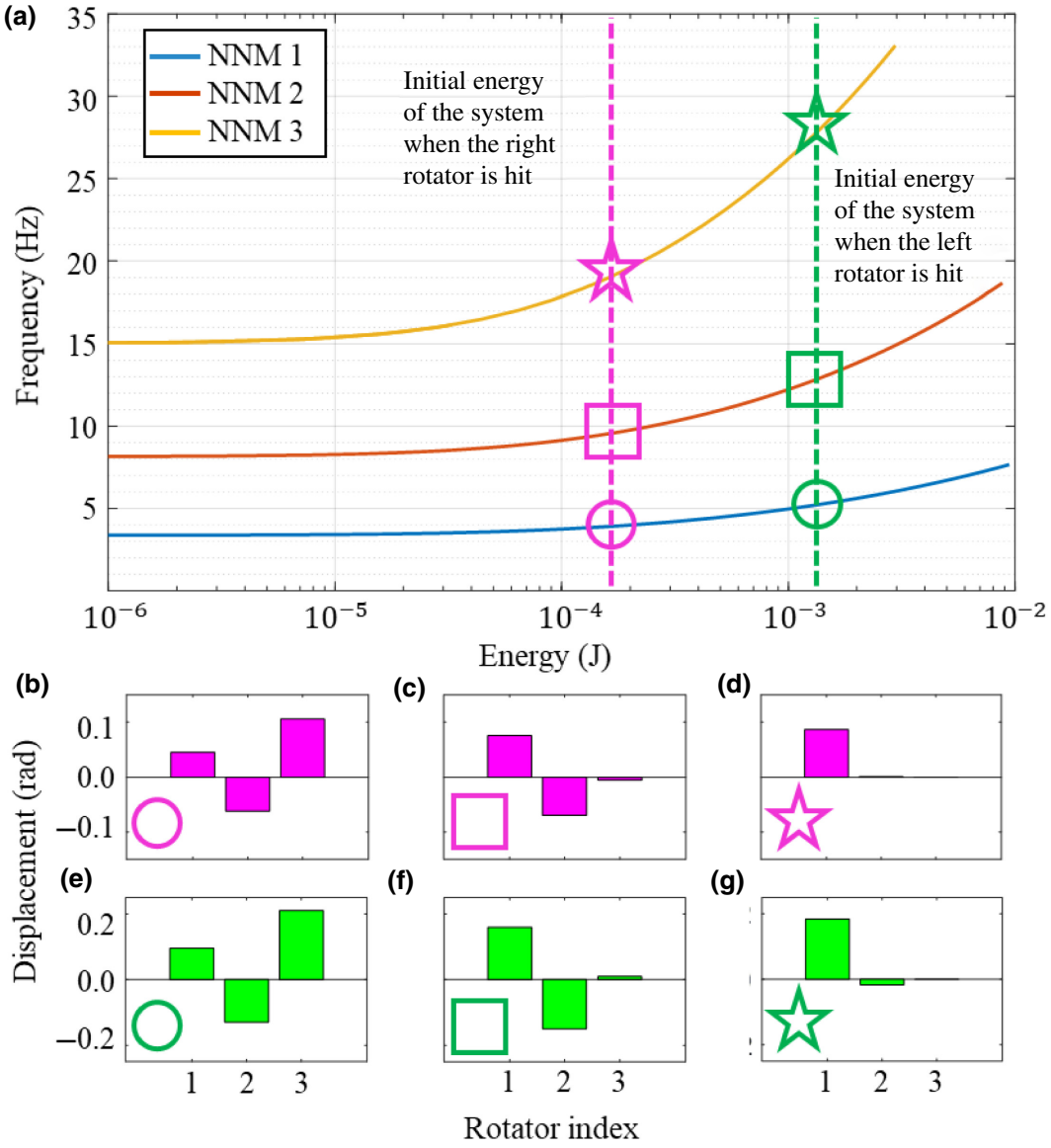


FIG. 3. (a) Computed nonlinear normal modes of the system. Two vertical dashed lines indicate the energy level of the system when one rotator is excited. (b)–(g) Nonlinear mode shapes corresponding to the markers in (a). Rotators 1, 2, and 3 represent the small, medium, and large rotators, respectively.

rotator under different excitation, whose horizontal axes are replaced by the instantaneous energy of the system (unlike Fig. 2, which uses time). The color of each frequency branch reveals the modal participation at this rotator. Note that the intensity of the frequencies vary from rotator to rotator, and thus the range of the color bars are not chosen to be identical. Similar to LNMs, the participation of each NNM reacts to the initial conditions. When the impulse is applied to the large rotator, we observe in Fig. 4(c) that most of this rotator's response is dominated by the first NNM. As documented in Figs. 4(a) and 4(b), the other two rotators exhibit response from all three NNMs, albeit it at lower amplitudes than observed in Fig. 4(c). When the impulse is applied to the small inertia rotator, however, we observe in Fig. 4(d) a very large modal participation in the third NNM for this rotator, while the large inertia shows a correspondingly small participation in this NNM as shown in Fig. 4(f). These results qualitatively match the mode shapes in Figs. 3(b)–3(g). In such a qualitative view, we show that, upon the same impulse excitation, as required by the reciprocity theorem, the response dynamics are distinct in both frequency and amplitude (mode shape).

Further, we show next that nonreciprocity still holds even if we seek an approximate solution of the system as a linear combination of the obtained NNMs, similar in spirit to the harmonic balance method. To this end, consider a combination of NNMs at the excitation energy level, with

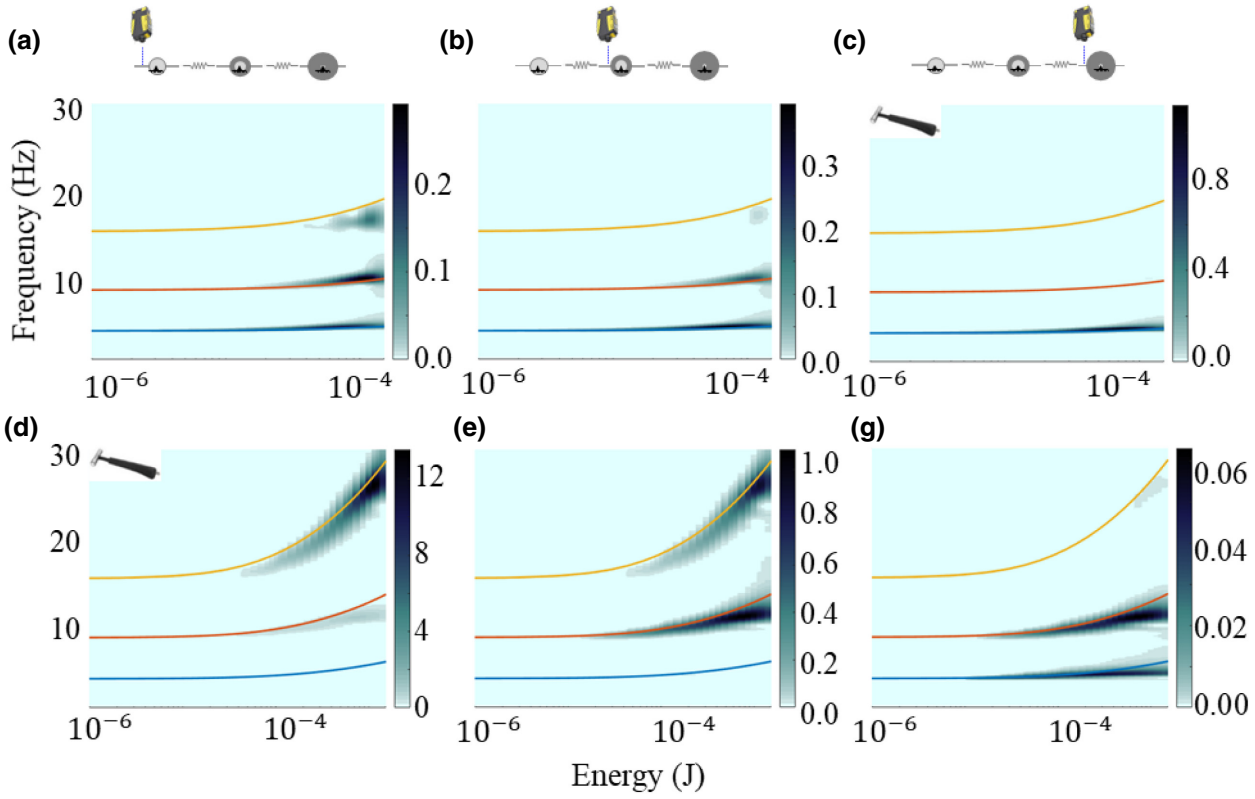


FIG. 4. Wavelet response of the impulse excitation superimposed with NNM results. (a)–(c) Wavelet response for each rotator when the impulse applies on the large rotator. (d)–(f) Wavelet response for each rotator when the impulse applies on the small rotator. Each column represents the corresponding rotator, e.g., the first column describes the response of the small rotator as indicated by the schematics on the top. The hammer symbol in (c) and (d) indicates the impulse excitation applies at this rotator.

the energy-dependent frequency $\omega$ and mode shapes $v$ provided in Table II.

We seek an approximate solution in the modal form,

$$x = C_1\mathbf{v}_1 \sin(\omega_1 t + \phi_1) + C_2\mathbf{v}_2 \sin(\omega_2 t + \phi_2) + C_3\mathbf{v}_3 \sin(\omega_3 t + \phi_3), \tag{13}$$

TABLE I. System parameter identification results.

| | Rotator 1 | Rotator 2 | Rotator 3 |
|---|---|---|---|
| Moment of inertia $I_i$ ( kg m$^2$) | $3.45 \times 10^{-6}$ | $1.28 \times 10^{-5}$ | $3.16 \times 10^{-5}$ |
| Dissipation coefficients $c_i$ (N ms) | $1.31 \times 10^{-5}$ | $8.7 \times 10^{-6}$ | $9.8 \times 10^{-6}$ |
| Dissipation coefficients $T_{if}$ (Nm) | $6.0 \times 10^{-7}$ | $3.18 \times 10^{-6}$ | $1.2 \times 10^{-6}$ |
| | Linkage 1 | Linkage 2 | |
| Stiffness $k_i$ (N/m) | 870 | 670 | |
| Undeformed length $L_i$ (mm) | 11.44 | 11.48 | |
| Gap distance $D_i$ (mm) | 11.74 | 11.84 | |

where $C_i$ and $\phi_i$ denote constants determined by the initial conditions,

$$\mathbf{x}(0)_l = 0,\ \dot{\mathbf{x}}(0)_l = \begin{Bmatrix} 0 \\ 0 \\ \frac{P r^*}{I_3} \end{Bmatrix}, \tag{14}$$

$$\mathbf{x}(0)_s = 0,\ \dot{\mathbf{x}}(0)_s = \begin{Bmatrix} \frac{P r^*}{I_1} \\ 0 \\ 0 \end{Bmatrix}. \tag{15}$$

In Eqs. (13)–(15) we convert the impulse excitation $P$ to into an equivalent initial velocity, $Pr^*/I_i$, with $r^*$ being the distance between the excitation point to the center of the rotator, and subscripts $l$ denotes the large inertia excitation and $s$ the small inertia excitation. Recall that the former initial condition results in a lower energy $E_1$ while the latter results in a higher energy $E_2$. After computing $C_1 \ldots C_3$ and $\phi_1 \ldots \phi_3$, we update Eq. (13) and present the receiving signal as

$$(x_1)_l = 0.0603 \sin(24.38t) - 0.0360 \sin(59.69t) + 0.0057 \sin(119.38t), \tag{16}$$

TABLE II. Frequency and mode shapes for each nonlinear normal mode at the excited energy.

| | $\omega_1$ (Hz) | $\omega_2$ (Hz) | $\omega_3$ (Hz) | $\mathbf{v}_1$ | $\mathbf{v}_2$ | $\mathbf{v}_3$ |
|---|---|---|---|---|---|---|
| Large Inertia Excitation | 3.88 | 9.50 | 19.00 | $\begin{bmatrix}-0.046\\0.062\\-0.106\end{bmatrix}$ | $\begin{bmatrix}-0.076\\0.070\\-0.005\end{bmatrix}$ | $\begin{bmatrix}-0.087\\-0.001\\0\end{bmatrix}$ |
| Small Inertia Excitation | 5.22 | 12.84 | 27.86 | $\begin{bmatrix}-0.096\\0.130\\-0.210\end{bmatrix}$ | $\begin{bmatrix}-0.159\\0.150\\-0.010\end{bmatrix}$ | $\begin{bmatrix}-0.184\\0.017\\0\end{bmatrix}$ |

$$(x_3)_s = 0.0084\sin(32.80t) - 0.0027\sin(80.68t) - 0.0003\sin(175.05t), \quad (17)$$

where $(x_1)_l$ represents the response of the small rotator at large inertia excitation, and $(x_3)_s$ the response of the large rotator under small inertia excitation. Clearly, reciprocity is broken, as these two responses exhibit significantly different modal amplitudes and frequencies, unlike that recovered by a similar procedure for a linear system where the responses would be identical. We also observe that the response in Eq. (16) has larger modal amplitudes for each mode, and lower oscillating frequencies, as compared to the response in Eq. (17), which qualitatively matches the experimental results in Figs. 2(c)–2(f).

## V. CONCLUDING REMARKS

In conclusion, we experimentally and numerically demonstrate nonreciprocal impulse response in an asymmetric in-plane rotator system, where tunable nonlinearity arises from prestretch of elastic linkages. We use a nonlinear normal-mode analysis to capture the major dynamics of the system and find a high degree of agreement between theory and experiment. A further analysis reveals that the same level of impulses applied on rotators with differing moments of inertia induce differing initial energy, which contributes to nonidentical oscillation frequency and dissimilar mode shapes, ultimately yielding nonreciprocal response.

The analysis of reciprocity breaking, informed by a NNM analysis, should be applicable to a large class of nonlinear, nonreciprocal systems where identical impulses induce asymmetrical energy input. Because of the simplicity of the proposed mechanical system, the structure can be easily modified as a nonlinear attachment to control waves in a linear wave guide, or tuned as a shock isolator, which protects targets from high-energy impacts while maintaining the energy transmission in the opposite direction. Future work aims to extend the structure to one-dimensional and two-dimensional periodic lattices and study its dynamical response subject to harmonic excitations.

## ACKNOWLEDGMENTS

The authors thank the National Science Foundation for partial support of this research under an Emerging Frontiers in Research and Innovation (EFRI) Grant No. 1741565.

## APPENDIX

### 1. Stiffness Expressions

The functional dependence of stiffness parameters appearing in Eqs. (10)–(12) are provided in Table AI.

TABLE A1. Stiffness expressions.

| | |
|---|---|
| $k_{g1}$ | $k_1 r(D_1 - L_1)$ |
| $k_{g2}$ | $k_1 r(D_1 - L_1) + k_2 r(D_2 - L_2)$ |
| $k_{g3}$ | $k_2 r(D_2 - L_2)$ |
| $k_{12}$ | $\dfrac{k_1 r^2 (D_1 - L_1)}{D_1}$ |
| $k_{23}$ | $\dfrac{k_2 r^2 (D_2 - L_2)}{D_2}$ |
| $\gamma_{g1}$ | $\dfrac{k_1 r}{3}\left(\dfrac{2r^2 L_1}{D_1^2} - r + \dfrac{2rL_1}{D_1} - \dfrac{D_1 - L_1}{2}\right)$ |
| $\gamma_{g2}$ | $\dfrac{k_1 r}{3}\left(\dfrac{2r^2 L_1}{D_1^2} - r + \dfrac{2rL_1}{D_1} - \dfrac{D_1 - L_1}{2}\right) + \dfrac{k_2 r}{3}\left(\dfrac{2r^2 L_2}{D_2^2} - r + \dfrac{2rL_2}{D_2} - \dfrac{D_2 - L_2}{2}\right)$ |
| $\gamma_{g3}$ | $\dfrac{k_2 r}{3}\left(\dfrac{2r^2 L_2}{D_2^2} - r + \dfrac{2rL_2}{D_2} - \dfrac{D_2 - L_2}{2}\right)$ |
| $\gamma_{12}^{+}$ | $\dfrac{k_1 r^2 L_1}{2D_1}\left(\dfrac{r^2}{D_1^2} + \dfrac{5r}{6D_1} + \dfrac{1}{6}\right)$ |
| $\gamma_{23}^{+}$ | $\dfrac{k_2 r^2 L_2}{2D_2}\left(\dfrac{r^2}{D_2^2} + \dfrac{5r}{6D_2} + \dfrac{1}{6}\right)$ |
| $\gamma_{12}^{-}$ | $\dfrac{k_1 r^2}{6}\left(1 - \dfrac{rL_1}{2D_1^2} - \dfrac{L_1}{2D_1}\right)$ |
| $\gamma_{23}^{-}$ | $\dfrac{k_2 r^2}{6}\left(1 - \dfrac{rL_2}{2D_2^2} - \dfrac{L_2}{2D_2}\right)$ |

[1] H. v. Helmholtz, Theorie der Luftschwingungen in Röhren mit offenen Enden, J. Reine Angew. Math. **57**, 1 (1860).

[2] J. Strutt, Some general theorems relating to vibrations, Proc. Lond. Math. Soc. **1**, 357 (1871).

[3] H. B. G. Casimir, On Onsager's principle of microscopic reversibility, Rev. Mod. Phys. **17**, 343 (1945).

[4] A. F. Vakakis, O. V. Gendelman, L. A. Bergman, D. M. McFarland, G. Kerschen, and Y. S. Lee, *Nonlinear Targeted Energy Transfer in Mechanical and Structural Systems* (Springer Science & Business Media, 2008), Vol. 156.

[5] A. Darabi and M. J. Leamy, Clearance-type nonlinear energy sinks for enhancing performance in electroacoustic wave energy harvesting, Nonlinear Dyn. **87**, 2127 (2017).

[6] K. J. Moore, J. Bunyan, S. Tawfick, O. V. Gendelman, S. Li, M. Leamy, and A. F. Vakakis, Nonreciprocity in the dynamics of coupled oscillators with nonlinearity, asymmetry, and scale hierarchy, Phys. Rev. E **97**, 012219 (2018).

[7] J. Li, X. Zhou, G. Huang, and G. Hu, Acoustic metamaterials capable of both sound insulation and energy harvesting, Smart Mater. Struct. **25**, 045013 (2016).

[8] C. Wang, S. Tawfick, and A. F. Vakakis, Irreversible energy transfer, localization and non-reciprocity in weakly coupled, nonlinear lattices with asymmetry, Physica D **402**, 132229 (2020).

[9] A. Darabi, L. Fang, A. Mojahed, M. D. Fronk, A. F. Vakakis, and M. J. Leamy, Broadband passive nonlinear acoustic diode, Phys. Rev. B **99**, 214305 (2019).

[10] B. Liang, X. Guo, J. Tu, D. Zhang, and J. Cheng, An acoustic rectifier, Nat. Mater. **9**, 989 (2010).

[11] B. Liang, B. Yuan, and J.-c. Cheng, Acoustic diode: rectification of acoustic energy flux in one-dimensional systems, Phys. Rev. Lett. **103**, 104301 (2009).

[12] R. Fleury, D. L. Sounas, C. F. Sieck, M. R. Haberman, and A. Alù, Sound isolation and giant linear nonreciprocity in a compact acoustic circulator, Science **343**, 516 (2014).

[13] Y. Chen, X. Li, H. Nassar, A. N. Norris, C. Daraio, and G. Huang, Nonreciprocal wave propagation in a continuum-based metamaterial with space-time modulated resonators, Phys. Rev. Appl. **11**, 064052 (2019).

[14] Z. Wu, Y. Zheng, and K. Wang, Metastable modular metastructures for on-demand reconfiguration of band structures and nonreciprocal wave propagation, Phys. Rev. E **97**, 022209 (2018).

[15] T. Devaux, A. Cebrecos, O. Richoux, V. Pagneux, and V. Tournat, Acoustic radiation pressure for nonreciprocal transmission and switch effects, Nat. Commun. **10**, 3292 (2019).

[16] Y. Li, C. Shen, Y. Xie, J. Li, W. Wang, S. A. Cummer, and Y. Jing, Tunable asymmetric transmission via lossy acoustic metasurfaces, Phys. Rev. Lett. **119**, 035501 (2017).

[17] J. Bunyan, K. J. Moore, A. Mojahed, M. D. Fronk, M. Leamy, S. Tawfick, and A. F. Vakakis, Acoustic nonreciprocity in a lattice incorporating nonlinearity, asymmetry, and internal scale hierarchy: Experimental study, Phys. Rev. E **97**, 052211 (2018).

[18] G. Trainiti, Y. Xia, J. Marconi, G. Cazzulani, A. Erturk, and M. Ruzzene, Time-periodic stiffness modulation in elastic metamaterials for selective wave filtering: Theory and experiment, Phys. Rev. Lett. **122**, 124301 (2019).

[19] L. Fang, A. Darabi, A. Mojahed, A. F. Vakakis, and M. J. Leamy, Broadband non-reciprocity with robust signal integrity in a triangle-shaped nonlinear 1D metamaterial, Nonlinear Dyn. **100**, 1 (2020).

[20] S. H. Mousavi, A. B. Khanikaev, and Z. Wang, Topologically protected elastic waves in phononic metamaterials, Nat. Commun. **6**, 8682 (2015).

[21] C. P. Wiederhold, D. L. Sounas, and A. Alù, Nonreciprocal acoustic propagation and leaky-wave radiation in a waveguide with flow, J. Acoust. Soc. Am. **146**, 802 (2019).

[22] H. Nassar, X. Xu, A. Norris, and G. Huang, Modulated phononic crystals: Non-reciprocal wave propagation and Willis materials, J. Mech. Phys. Solids **101**, 10 (2017).

[23] G. Trainiti and M. Ruzzene, Non-reciprocal elastic wave propagation in spatiotemporal periodic structures, New J. Phys. **18**, 083047 (2016).

[24] J. Li, C. Shen, X. Zhu, Y. Xie, and S. A. Cummer, Nonreciprocal sound propagation in space-time modulated media, Phys. Rev. B **99**, 144311 (2019).

[25] X. Zhu, J. Li, C. Shen, X. Peng, A. Song, L. Li, and S. A. Cummer, Non-reciprocal acoustic transmission via space-time modulated membranes, Appl. Phys. Lett. **116**, 034101 (2020).

[26] L. Quan, D. L. Sounas, and A. Alù, Nonreciprocal Willis coupling in zero-index moving media, Phys. Rev. Lett. **123**, 064301 (2019).

[27] B.-I. Popa and S. A. Cummer, Non-reciprocal and highly nonlinear active acoustic metamaterials, Nat. Commun. **5**, 3398 (2014).

[28] N. Boechler, G. Theocharis, and C. Daraio, Bifurcation-based acoustic switching and rectification, Nat. Mater. **10**, 665 (2011).

[29] E. Rivet, A. Brandstötter, K. G. Makris, H. Lissek, S. Rotter, and R. Fleury, Constant-pressure sound waves in non-Hermitian disordered media, Nat. Phys. **14**, 942 (2018).

[30] H. Nassar, B. Yousefzadeh, R. Fleury, M. Ruzzene, A. Alù, C. Daraio, A. N. Norris, G. Huang, and M. R. Haberman, Nonreciprocity in acoustic and elastic materials, Nat. Rev. Mater. **5**, 667 (2020).

[31] C. Coulais, D. Sounas, and A. Alù, Static non-reciprocity in mechanical metamaterials, Nature **542**, 461 (2017).

[32] Z. Lu and A. N. Norris, Non-reciprocal wave transmission in a bilinear spring-mass system, J. Vib. Acoust. **142**, 021006 (2020).

[33] A. Mojahed and A. F. Vakakis, Certain aspects of the acoustics of a strongly nonlinear discrete lattice, Nonlinear Dyn. **99**, 643 (2020).

[34] K. L. Manktelow, M. J. Leamy, and M. Ruzzene, Weakly nonlinear wave interactions in multi-degree of freedom periodic structures, Wave Motion **51**, 886 (2014).

[35] A. Darabi and M. Leamy, Weakly and Strongly Nonlinear Periodic Materials: Tunable Dispersion, Non-Reciprocity, and Device Implications, Nonlinear Vibrations, Localization and Energy 58.

[36] A. Blanchard, T. P. Sapsis, and A. F. Vakakis, Non-reciprocity in nonlinear elastodynamics, J. Sound Vib. **412**, 326 (2018).

[37] O. Gendelman, V. Zolotarevskiy, A. Savin, L. Bergman, and A. Vakakis, Accelerating oscillatory fronts in a nonlinear sonic vacuum with strong nonlocal effects, Phys. Rev. E **93**, 032216 (2016).

[38] O. Rudenko and E. Solodov, Strongly nonlinear shear perturbations in discrete and continuous cubic nonlinear systems, Acoust. Phys. **57**, 51 (2011).

[39] Z. Zhang, L. I. Manevitch, V. Smirnov, L. A. Bergman, and A. F. Vakakis, Extreme nonlinear energy exchanges in a geometrically nonlinear lattice oscillating in the plane, J. Mech. Phys. Solids **110**, 1 (2018).

[40] See Supplemental Material at http://link.aps.org/supplemental/10.1103/PhysRevApplied.15.034005 for external discussion on periodic structure, experimental parameter identification, and effects of imperfect excitation.

[41] S. Shaw and C. Pierre, Non-linear normal modes and invariant manifolds, J. Sound Vib. **150**, 170 (1991).

[42] S. W. Shaw and C. Pierre, Normal modes for non-linear vibratory systems, J. Sound Vib. **164**, 85 (1993).

[43] G. Kerschen, M. Peeters, J.-C. Golinval, and A. F. Vakakis, Nonlinear normal modes, Part I: A useful framework for the structural dynamicist, Mechanical Systems and Signal Processing, Mech. Syst. Signal Process. **23**, 170 (2009).

[44] M. Peeters, R. Viguié, G. Sérandour, G. Kerschen, and J.-C. Golinval, Nonlinear normal modes, Part II: Toward a practical computation using numerical continuation techniques, Mech. Syst. Signal Process. **23**, 195 (2009).

[45] J. C. Slater, A numerical method for determining nonlinear normal modes, Nonlinear Dyn. **10**, 19 (1996).